ADVANCED ENGINEERING MATERIALS

DOI: 10.1002/adem.201500151

Ultrafine Grained Structures Resulting from SPD-Induced Phase Transformation in Al–Zn Alloys**

By *Xavier Sauvage,* Maxim Yu. Murashkin, Boris B. Straumal, Elena V. Bobruk* and *Ruslan Z. Valiev*

Three different Al–Zn alloys (2, 10, 30 wt% Zn) have been processed by severe plastic deformation (SPD) in the solutionized state to investigate the concomitant mechanisms of grain refinement and phase separation. The data of high resolution analytical transmission electron microscopy clearly reveal the key role of grain boundaries that promote Zn segregation and fast diffusion. Surprisingly, it is also shown that SPD carried out at 150 °C could give rise to a finer multiphase structure comparing to room temperature processing. Our observations seem to indicate that it resulted from a competition between the classical discontinuous precipitation of Zn and SPD-induced dynamic precipitation.

1. Introduction

During the past 20 years, a large proportion of the research devoted to ultrafine grained (UFG) alloys processed by severe plastic deformation (SPD) has been devoted to aluminum alloys. All these efforts have been pushed by various motivations obtaining super-plastic properties, improving the combination of strength and electrical conductivity or achieving higher strength by grain refinement eventually combined with solid solution or precipitate hardening. Attempts have been tried on most of commercially available aluminum alloys using the most common SPD processes like high pressure torsion (HPT), equal channel angular pressing (ECAP), or accumulative roll bonding (ARB) (see refs.[1–4] for some reviews). The grain refinement achieved by such techniques is typically in a range of 1 μm to 100 nm giving rise to a strong strengthening as predicted by the Hall and Petch law[5–8] and even sometimes with a larger increase.[9] Besides, the combination of small grains with a fine distribution of nanoscaled precipitates seems an attractive route as it has also been shown that it may significantly increase both the yield stress as well as ductility.[10,11] However, controlling the precipitation in UFG structures is challenging because of the concomitant recovery, grain growth, and recrystallization phenomena. Moreover, heterogeneous precipitation along dislocations or grain boundaries (GBs) is also very likely to occur[12,13] and a fastest precipitation kinetic along with a modified precipitation sequence may appear.[14] Some authors have tried to carry out grain refinement by SPD at a temperature close or slightly below the classical aging temperature to achieve both processes at the same time.[12,15–18] But under such conditions, the final microstructures are also difficult to control because of the strong interaction between defects and solute atoms. It has even been demonstrated that in some binary systems, namely Al–Cu[19] and Al–Zn,[20–23] the quenched supersaturated solid solutions are destabilized during SPD at room temperature

[*] *Dr. X. Sauvage*
Groupe de Physique des Matériaux, UMR CNRS 6634, Université et INSA de Rouen, 76801, Saint Etienne du Rouvray, France
E-mail: xavier.sauvage@univ-rouen.fr
Dr. M. Y. Murashkin, Dr. E. Bobruk, Dr. R. Z. Valiev
Institute of Physics of Advanced Materials, Ufa State Aviation Technical University, K. Marx str. 12, Ufa 45000, Russia
Dr. B. B. Straumal
Moscow Institute of Physics and Technology (State University), Institutskii per. 9, 141700 Dolgoprudny, Russia
Dr. B. B. Straumal
Laboratory of Hybrid Nanomaterials, National University of Science and Technology "MISIS", Leninskii prosp. 4, 119049 Moscow, Russia
Institute of Solid State Physics, Russian Academy of Sciences, 142432 Chernogolovka, Russia
Dr. R. Z. Valiev
Research Laboratory for Mechanics of New Nanomaterials, Saint Petersburg State Polytechnical University, Saint Petersburg 195251, Russia

[**] *Prof. David Embury is acknowledged by XS for the fruitful discussions on discontinuous precipitation and atomic transport promoted by SPD. The work was partially supported by the Russian Foundation for Basic Research (grant 14-03-31510), the Ministry of Education and Science of the Russian Federation (in the framework of Increase Competitiveness Program of MISiS and for the grant 14.A12.31.0001 as well as through the Russian Program "5-100-2020" for RZV).*

(RT) leading to the nucleation and growth of a large density of precipitates. It has been proposed that the atomic mobility could be significantly enhanced during SPD especially thanks to the high vacancy concentration,[24–30] solute drag by dislocations,[31,32] pipe diffusion along dislocations,[33] or grain boundary diffusion.[34,35] In the present work, we have systematically investigated such dynamic precipitation phenomena in a series of Al–Zn alloys with various Zn content and at different processing temperature. The Al–Zn phase diagram[36] is relatively simple with no stable intermetallic phase and a relatively equilibrium mutual solubility near room temperature. Thus, face-centred cubic (fcc) non-equilibrium supersaturated solid solutions quenched from the high temperature solubility range typically decompose in two phases, namely the fcc Al and hexagonal closely packed (hcp) Zn phases. On the Al-rich side of the phase diagram, if the Zn concentration is well below 10 at%, Guinier–Preston (G.P.) zones form at first, followed by the fcc metastable α' phase and finally the hcp Zn.[37]

However, if the Zn concentration is higher, then the supersaturated solid solution typically decomposes into a lamellar mixture of Al and Zn phases through a discontinuous precipitation (DP) process (or cellular reaction).[38–41] This solid state reaction transforms the solid solution into the two phases aggregate behind a migrating reaction front along which solute atoms are easily redistributed.[42] Such a two-phase lamellar structure is very similar to that formed in the eutectic or eutectoid decomposition reaction.[38–41] It is important to note that in the Al–Zn system, the velocity of this reaction front depends both on composition and temperature.[38] Besides, for Zn contents between 20 and 50 at%, it has been reported that a spinodal decomposition of the solid solution may occur.[43,44] Thus, the aim of the present work was to set this system under different transformation conditions (composition and temperature) during SPD (which is known to promote the decomposition) for a better understanding of deformation-induced precipitation mechanisms and the links with structure refinement.

2. Experimental Section

Three different alloys with different Zn content were prepared for the present study, namely Al–2Zn, Al–10Zn, and Al–30Zn (wt%). It is important to note that for these compositions, spinodal decomposition is not expected.[43] These alloys were obtained from high purity components (5N Al and 5N5 Zn) by vacuum induction melting. After casting, the alloys were homogenized at 500 °C. Disc-shaped samples with a diameter of 20 mm and a thickness of 1.4 mm were cut out for SPD processing using HPT. Materials were always solutionized at 500 °C, followed by water quenching immediately before HPT processing. The HPT process was carried out with a pressure of 6 GPa and an anvil revolution speed of one turn per minute. Samples were deformed up to 10 revolutions at room temperature or 150 °C. The temperature was controlled by heating the anvils prior to deformation, and samples were pressed without shear deformation during few minutes to stabilize their temperature.

Microstructure characterizations were performed always at the same location in HPT discs, at a distance of 5 mm from the center, corresponding to a shear strain of about 300. Samples for the transmission electron microscopy (TEM) were prepared using standard electropolishing methods (30 vol% HNO_3 in methanol, temperature –35 °C, voltage 20 V) and were observed with a probe-corrected ARM200F JEOL microscope operated at 200 kV. Images were recorded in the scanning mode in scanning transmission electron microscopy (STEM) with a probe size of 0.2 nm and a convergence angle of 34 mrad. Both bright field (BF) and high-angle annular dark field (HAADF) detectors with collection angles in the range of 80–300 mrad were used for this investigation. To quantify the local Zn concentrations, energy-dispersive X-ray spectroscopy (EDS) was performed using a JEOL JED2300 detector. Atom probe tomography (APT) samples were also prepared by standard electropolishing techniques.[45] Analyses were performed in ultrahigh vacuum conditions, using an energy-compensated atom probe equipped with an advanced delay line detector (ADLD)[46] and a reflectron. Samples were field evaporated at 30 K using electric pulses (30 kHz pulse repetition rate and 20% pulse fraction).

3. Results and Discussion

3.1. Influence of the Zn Concentration (Driving Force for Precipitation)

As reported in earlier works from us[20–22,47] or others,[23] it was not surprising to achieve a full decomposition of the quenched supersaturated solid solution in the Al–10Zn alloy during HPT. As revealed by STEM-BF images (Figure 1a), the mean grain size after HPT is about 1 μm and large Zn particles have nucleated and grown along GBs and triple lines. The size of these particles is large, in a range of 100–300 nm. There is also a low density of smaller particles located inside the grains (Figure 1a and b). Also, like in our earlier work,[21,47] some GB Zn segregations were often observed (Figure 1b and c) with amplitudes varying from few at% up to about 10% in some cases. The EDS line profile of Figure 1c was performed across both a nanoscale particle and a GB. The particle being embedded in the Al matrix, the local Zn concentration measured by EDS is well below the real value. It shows, however, a good correspondence between the Zn concentration and the recorded HAADF signal. It is interesting to note that the Zn concentration in the matrix is down to 2 at% after HPT, i.e., very close to the equilibrium solubility limit reported in the literature[36] and a local concentration of Zn up to about 4 at% is measured at the GB. Without deformation and if the alloy is kept at room temperature, only the nucleation of G.P. zones is expected.[37] Thus, one may assume that the observed decomposition of the solid solution with

ADVANCED ENGINEERING MATERIALS

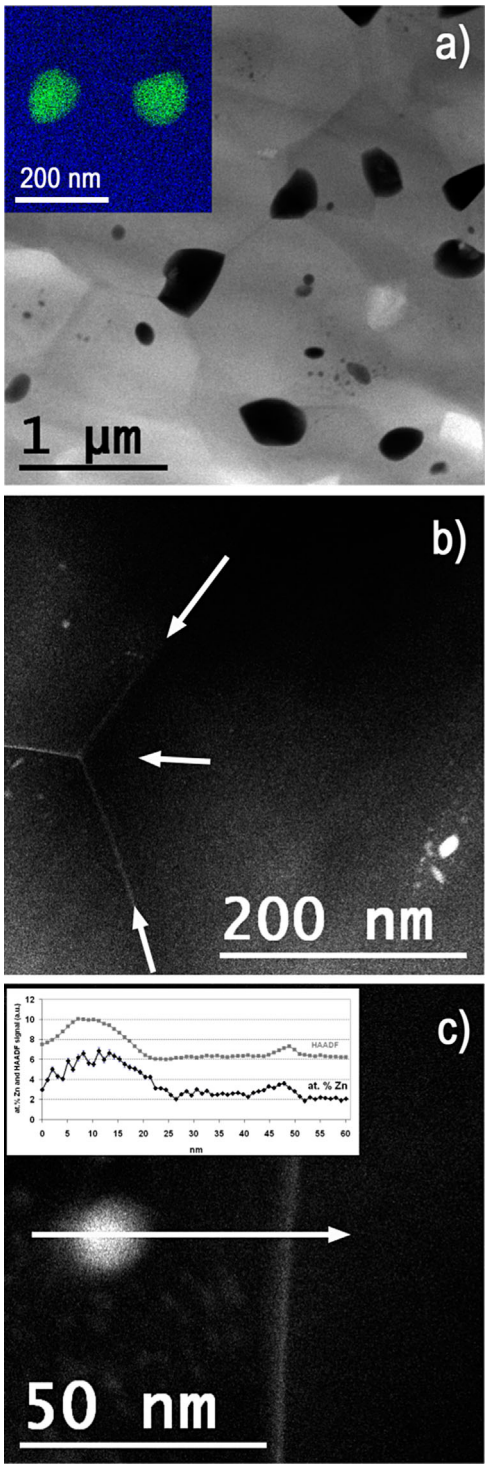

Fig. 1. Microstructure of the Al–10Zn alloy processed by HPT (10 revolutions) at RT. (a) STEM-BF image showing that the mean grain size is about 1 μm and that large Zn-rich particles have nucleated at GBs and triple lines (darkly imaged and confirmed by the EDS map [inset, with Al-K blue and Zn-K green]). (b) STEM-HAADF image showing the evidence of Zn grain boundary segregation (GBs are arrowed). (c) STEM-HAADF image of a nanoscaled precipitate and a GB enriched in Zn (confirmed by the EDS line profile along the arrow, see inset).

the formation of extremely large Zn particles could be the result of a temperature increase during the deformation. Such temperature increase may originate not only from the plastic deformation but also from the exothermic phase transformation itself. Yang and coworkers have indeed measured in an Al–59.5Zn alloy transformed in an oil bath a temperature increase up to 30 K. As for the temperature increase due to the plastic work, it has been shown by Edalati *et al.* that it is typical not more than 10 or 20 K in the HPT conditions used in the present study because of the strong heat transfer between the sample and the anvils during the process.[48]

To check that in the present case, the observed phase transformation is mainly deformation driven; the Al–2Zn alloy was prepared and deformed in similar HPT conditions. The Zn content of this alloy is very close to the solubility limit at room temperature;[36] however, as shown in Figure 2a, few nanoscaled precipitates have nucleated inside grains during SPD. Most of these precipitates are facetted, and exhibit the typical morphology of the semi-coherent metastable fcc α' phase particles (Figure 2c). The Zn concentration was too low to give rise to the nucleation and growth of precipitates at triple lines and along GBs. It was also impossible to detect any significant Zn segregation along GBs. These two features probably explain the larger grain size after HPT comparing to the Al–10Zn alloy (in a range of 1–2 μm, Figure 2a) because of the absence of pinning. However, the most important is that if a significant temperature increase would have occurred during the HPT process, it would have pushed the solid solution into a stable domain and precipitation inside grains would not have occurred. Indeed, for example, the equilibrium solubility of Zn in Al is about 4 at% at 400 K only.[36] Thus, this experiment clearly demonstrates that there is no significant heating during the HPT process thanks to the efficient heat transfer through the anvils.

When the Zn content is increased up to 30 wt%, the volume fraction of large Zn particles at triple lines and GBs is also increased (Figure 3a). There is also a larger density of intragranular nanoscaled particles (Figure 3a and b), and as revealed for the Al–10Zn alloy, there is some significant Zn grain boundary segregations (Figure 3b).

The density of GB pining media (particles and GB segregations) being larger, it is not surprising to observe significantly smaller Al grains as compared to the Al–10Zn (down to about 500 nm, see Figure 3a). The amount of Zn detected along GBs seems higher, but it is difficult to quantify it precisely as it spreads in a large range. As discussed in an earlier work, it is linked to the contact angle of the Zn particles[21,47] and also probably to the local specific structure of the GBs resulting from the SPD process.[1,49] Like in the Al–Mg system,[50] these segregations are most probably the result of the large vacancy concentration continuously created during SPD.[24–29] They diffuse toward GBs where they annihilate, and since they exhibit a positive binding energy with Zn atoms, this vacancy flux creates a Zn flux toward GBs. Then, the high mobility of Zn atoms along GBs is believed to lead to the fast growth of Zn particles located at triple junctions. The interesting point is that in such a process, the Zn content does not seem to play a significant role. Of course, it directly affects the volume fraction of Zn phase that

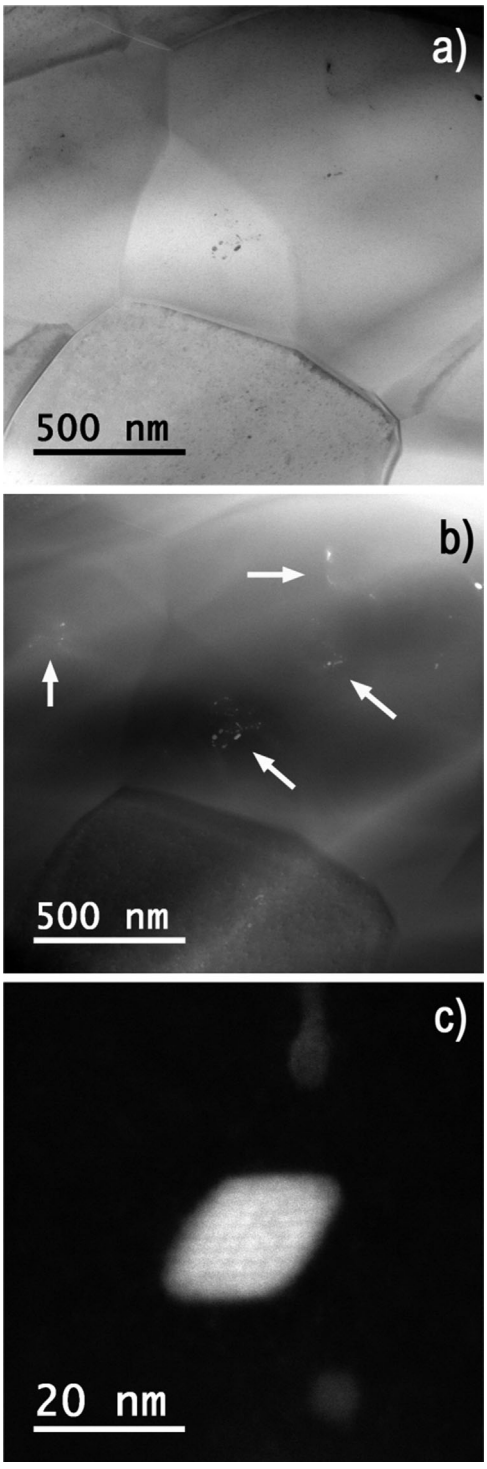

Fig. 2. Microstructure of the Al–2Zn alloy processed by HPT (10 revolutions) at RT. (a) STEM-BF image showing that the grain size is about 1 μm. (b) STEM-HAADF image showing few nanoscaled Zn-rich precipitates (arrowed) that have nucleated during deformation in the grain interior. (c) STEM-HAADF image showing a nanoscaled facetted α′ Zn-rich precipitate semi-coherent with the fcc Al matrix.

appears at the end of the transformation, but the coarsening rate of Zn particles is so large that recovery processes and the GB mobility is not very much affected which gives rise to large grain sizes even for Zn concentration up to 30 wt%.

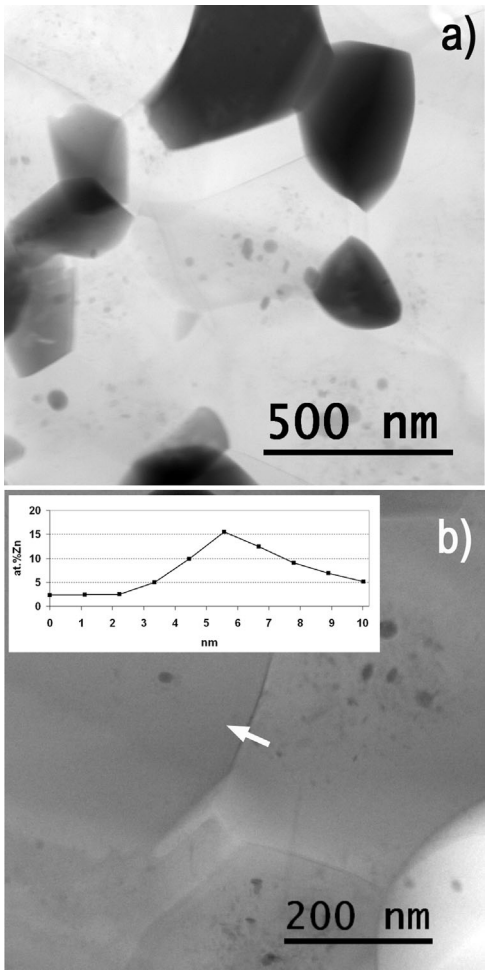

Fig. 3. Microstructure of the Al–30Zn alloy processed by HPT (10 revolutions) at RT. (a) STEM-BF image showing that the mean grain size is about 500 nm and that large Zn-rich particles (darkly imaged) have nucleated at GBs and triple lines. There are also few nanoscaled Zn-rich precipitates in the grain interiors. (b) STEM-BF image showing Zn segregation along a GB, as confirmed by the EDS line profile (inset).

3.2. Influence of the Processing Temperature

When the Al–30Zn alloy is deformed by HPT at 150 °C (Figure 4), the microstructure appears very different comparing to the RT process (Figure 3). There are still some large Zn particles at triple lines and along GBs but less numerous (Figure 4a). Most surprisingly, the intragranular particle number density is much higher (Figure 4b and c). Some of them are facetted α′ particles, but others that are mainly located in the vicinity of GBs look like fragmented ribbons (Figure 4b and d). The Zn content in the fcc Al matrix was measured both using EDS analysis in the TEM (5 ± 0.5 at%) and APT (6 ± 0.5 at%). The slight discrepancy might be attributed to the low statistic of APT analyses where only very small volumes are probed. As expected, it is much higher than in the same material processed at RT (2.5 ± 0.5 at%), and it is in good agreement with the equilibrium solubility of Zn in fcc Al.[36] Thus, again at this temperature the decomposition of the supersaturated solid solution was completely achieved during the SPD process. One should note that no Zn segregation along GBs could be observed in this state and also that the mean grain

ADVANCED ENGINEERING MATERIALS

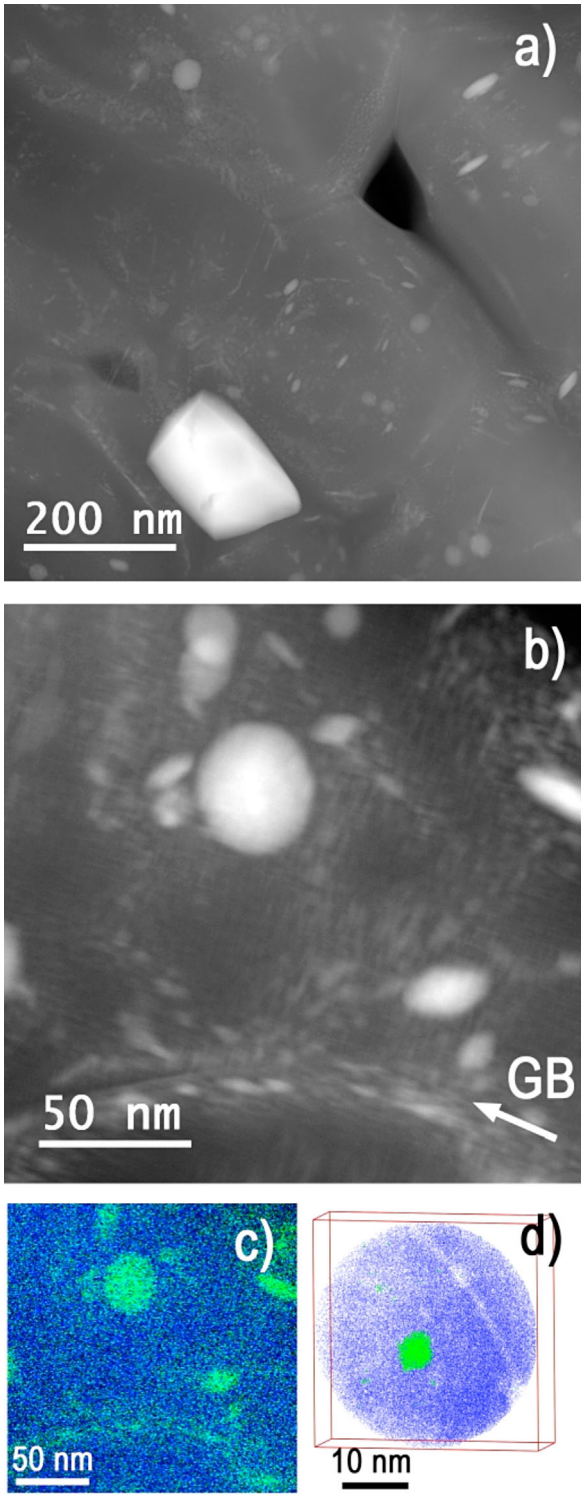

Fig. 4. Microstructure of the Al–30Zn alloy processed by HPT (10 revolutions) at 150 °C. (a) STEM-HAADF image showing that large Zn-rich particles (brightly imaged) have nucleated at triple lines but also a large density of smaller precipitates in the grain interior. (b) STEM-HAADF image showing the nanoscaled precipitates in the GB region (arrowed). (c) EDS map (Al-K blue and Zn-K green) corresponding to (b). (d) 3D reconstruction of a volume analyzed by APT and containing a nanoscaled facetted α′ Zn rich precipitate (filtered image showing only Zn atoms where the local Zn concentration is higher than 20 at%).

size is just slightly higher than in the material processed at RT (about 600 nm vs. 500 nm). This is rather surprising as dynamic recovery mechanisms should be much more active at this temperature, but the high density of nanoscaled precipitate and the higher solute content seem to be rather effective in pinning boundaries.

During any precipitation treatment, it is well accepted that a lower temperature gives rise to smaller particles as the driving force for transformation is larger and the atomic mobility lower. In the present case, for the SPD induced nucleation and growth of Zn particles, the situation is surprisingly reversed: a higher number density of smaller particles is observed in the alloy transformed at 150 °C (Figure 4) comparing to RT (Figure 3). However, it should be noted that in the Al–Zn system, when the Zn concentration is large enough, the supersaturated solid solution transforms via a DP process[38–41] and the kinetic of the reaction is controlled by the velocity of the reaction front along which solute atoms are easily redistributed to form the two phase lamellar mixture.[42] The kinetic of such a reaction is both composition and temperature dependent and could also be affected by a prior plastic deformation. Indeed, Boumerzoug *et al*. have shown that after 45% reduction by cold rolling, the DP reaction in an Al–30Zn alloy was retarded or even inhibited, since dislocations offer a large density of nucleation sites for the nucleation of intragranular particles.[41] In our case, the situation is, however, different because as discussed above, there is a continuous flow of Zn atoms toward GBs during SPD leading to GB segregations and a fast growth of particles at triple lines. However, when the temperature is above room temperature, this process has to compete with the classical DP reaction. Indeed, it has been demonstrated that the velocity of this reaction front is almost two orders of magnitude higher at 150 °C than at room temperature.[38] However, it is important to note that during SPD, GBs also move. It has been recently experimentally proved by Renk and coworkers.[51] The estimation of the mean GB velocity V during the HPT process can be estimated using a simple geometric model[52] and may be written as

$$V_{GB} = d\,A\,(f-1)^{1/2}/f^{3/2} \quad (1)$$

where d is the mean grain size, f is the average grain shape aspect ratio, and A the shear strain rate ($A \sim 0.5\ s^{-1}$ in the present study).

This means that GB velocity during SPD is compared to the velocity of the DP reaction front in Figure 5a for a large range of grain sizes and grain aspect ratio. It clearly shows that at room temperature, the GB motion is much faster making any DP impossible. However, at 150 °C, the velocity of the DP reaction front is very close to the mean GB velocity, and then it should lead to a competition between the two transformation mechanisms. The differences between the decomposition of the solid solution at RT and at 150 °C are schematically represented and summarized in Figure 5b and c. On these

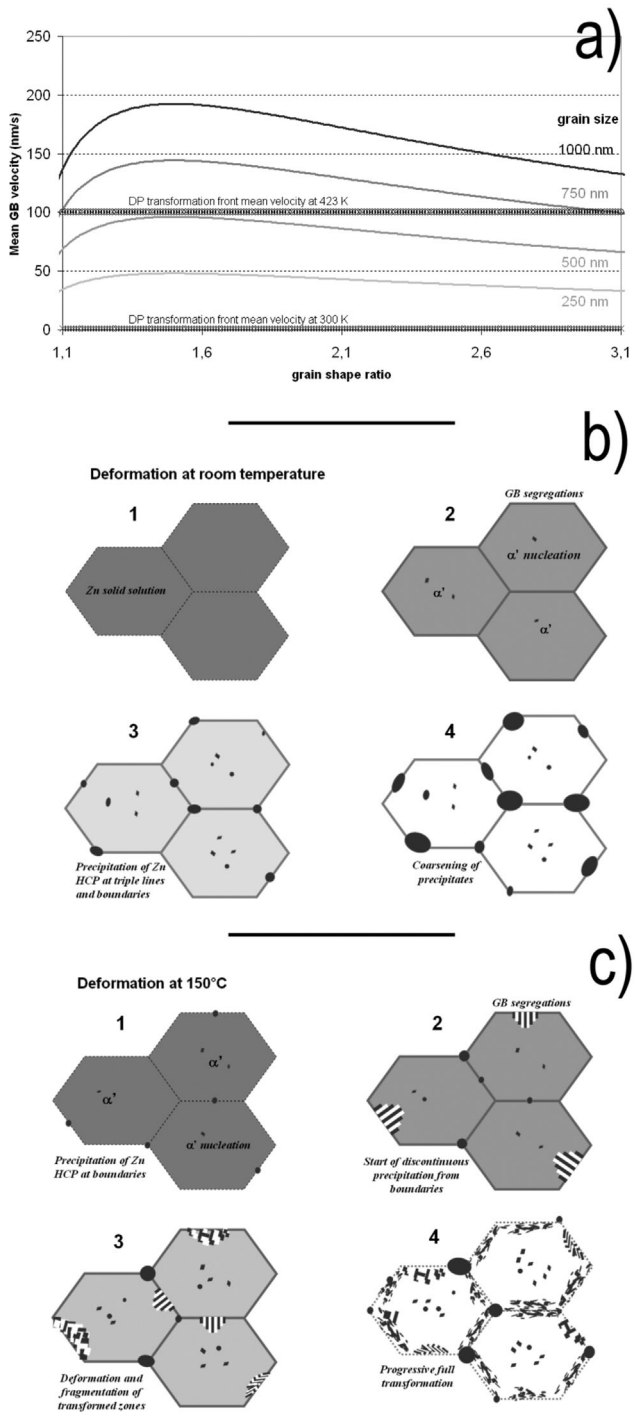

Fig. 5. (a) Estimated mean velocity of GBs during the HPT process as a function of the grain size and shape ratio (see text for details) compared to the mean velocity of the transformation front of the DP at RT and 150 °C (from ref.[38]). (b) Schematic representation of the phase separation process induced by SPD at RT. (c) Schematic representation of the phase separation process induced by SPD at 150 °C where the DP simultaneously occurs. For these schematic representations, steps 1–4 correspond to an increase of plastic deformation. Step 1 is for the early stage where the UFG structure is formed but the decomposition has not already started. Step 4 is the final state observed in the present work. The gray level was modulated to account for the change of Zn in solid solution (dark gray for higher concentration).

schematic representations, the different steps from one to four correspond to an increasing level of deformation. The first step is not the initial coarse-grained material but the early stage of deformation where the UFG starts to form but when the supersaturated solution is not decomposed. The last step corresponds to our observations. In between, one should note that the grain size and shape were kept constant only for the sake of simplicity as we focus here mainly on the phase transformation mechanisms. At 150 °C, during the deformation, some DP may start along some GBs (step 2, Figure 5c), but then during the continuous deformation process, the resulting lamellar structure gets fragmented while DP eventually starts along other GBs (step 3, Figure 5c). At the end, the solid solution is fully decomposed and in the vicinity of GBs there is a high density of fragmented Zn lamellae as observed experimentally (Figure 4b and c). Since the influence of the level of plastic deformation was not investigated in the present work, the level of plastic deformation required to reach each step is unknown. Further studies are planned in the near future to clarify this point and also to find out if the observed states (step 4) correspond to a steady state or if further microstructure evolution could occur.

4. Conclusions

The Al–Zn system turns out to be a very interesting model system to study phase transformations induced by SPD and their link with grain size refinement mechanisms. By varying the alloy composition and the processing parameters, it was found that

1. The fast and complete decomposition of Al–Zn solid solutions during SPD is mainly deformation driven and does not seem to result from an increase of the local temperature during the HPT process.
2. The decomposition of quenched supersaturated solid solutions occurs via the nucleation of semi-coherent meta-stable fcc α' particles inside grains and the segregation of Zn atoms to GBs where they promote the fast growth of Zn particles at triple junctions.
3. The Zn content only affects the final volume fraction of Zn-rich phase as expected by the phase diagram.
4. When the HPT temperature is increased from RT to 150 °C, a higher number density of smaller Zn-rich particles is formed. They slow down dynamic recovery processes and lead to a grain size rather similar for both temperatures.
5. The much higher precipitate density measured at 150 °C is attributed to a competition between the classical DP process and SPD decomposition observed at lower temperature.

Article first published online: May 19, 2015
Manuscript Revised: April 24, 2015
Manuscript Received: March 20, 2015

[1] R. Z. Valiev, *Mater. Sci. Forum* **2008**, *584–586*, 22.
[2] R. Z. Valiev, R. K. Islamgaliev, I. V. Alexandrov, *Prog. Mater. Sci.* **2000**, *45*, 103.

[3] R. Z. Valiev, T. G. Langdon, *Prog. Mater. Sci.* **2006**, *51*, 881.
[4] Y. Estrin, A. Vinogradov, *Acta Mater.* **2013**, *61*, 782.
[5] C. Pande, K. Cooper, *Prog. Mater. Sci.* **2009**, *54*, 689.
[6] F. Louchet, J. Weiss, T. Richeton, *Phys. Rev. Lett.* **2006**, *97*, 75504.
[7] E. O. Hall, *Proc. Phys. Soc.* **1951**, *B 64*, 747.
[8] N. J. Petch, *J. Iron Steel Inst.* **1953**, *173*, 25.
[9] R. Z. Valiev, N. A. Enikeev, M. Yu. Murashkin, V. U. Kazykhanov, X. Sauvage, *Scr. Mater.* **2010**, *63*, 949.
[10] S. Cheng, Y. H. Zhao, Y. T. Zhu, E. Ma, *Acta Mater.* **2007**, *55*, 5822.
[11] E. Ma, *JOM* **2006**, *58*, 49.
[12] X. Sauvage, M. Yu. Murashkin, R. Z. Valiev, *Kovove Mater. Metal. Mater.* **2011**, *49*, 11.
[13] A. Cerri, P. Leo, *Mater. Sci. Eng. A* **2005**, *410–411*, 226.
[14] A. Deschamps, F. de Geuser, Z. Horita, S. Lee, G. Renou, *Acta Mater.* **2014**, *66*, 105.
[15] R. Z. Valiev, M. Yu. Murashkin, I. Sabirov, *Scr. Mater.* **2014**, *76*, 13.
[16] G. Sha, K. Tugcu, X. Z. Liao, *Acta Mater.* **2014**, *63*, 169.
[17] G. Sha, Y. B. Wang, X. Z. Liao, Z. C. Duan, S. P. Ringer, T. G. Langdon, *Acta Mater.* **2009**, *57*, 3123.
[18] Z. Horita, K. Ohashi, T. Fujita, K. Kaneko, T. G. Langdon, *Adv. Mater.* **2005**, *17*, 1599.
[19] A. Hohenwarter, M. Faller, B. Rashkova, R. Pippan, *Phil. Mag. Lett.* **2014**, *94*, 342.
[20] N. Q. Chinh, R. Z. Valiev, X. Sauvage, G. Varga, K. Havancsák, M. Kawasaki, B. B. Straumal, T. G. Langdon, *Adv. Eng. Mater.* **2014**, *16*, 1000.
[21] B. B. Straumal, X. Sauvage, B. Baretzky, A. A. Mazilkin, R. Z. Valiev, *Scr. Mater.* **2014**, *70*, 59.
[22] B. B. Straumal, B. Baretzky, A. A. Mazilkin, F. Philipp, O. A. Kogtenkova, M. N. Volkov, R. Z. Valiev, *Acta Mater.* **2004**, *52*, 4469.
[23] A. Alhamidi, K. Edalati, Z. Horita, S. Hirosawa, K. Matsuda, D. Terada, *Mater. Sci. Eng. A* **2014**, *610*, 17.
[24] D. Setman, E. Schafler, E. Korznikova, M. Zehetbauer, *Mater. Sci. Eng. A* **2008**, *4923*, 116.
[25] S. Van Petegem, F. Dalla Torre, D. Segers, H. Van Swygenhoven, *Scr. Mater.* **2003**, *48*, 17.
[26] R. Würschum, W. Greiner, R. Z. Valiev, M. Rapp, W. Sigle, O. Schneeweiss, H. Schaefer, *Scr. Metall.* **1991**, *25*, 2451.
[27] G. Saada, *Physica* **1961**, *27*, 657.
[28] A. L. Ruoff, R. W. Balluffi, *J. Appl. Phys.* **1963**, *34*, 2862.
[29] H. Mecking, Y. Estrin, *Scr. Metall.* **1980**, *14*, 815.
[30] K. Oh-ishi, K. Edalati, H. S. Kim, K. Hono, Z. Horita, *Acta Mater.* **2013**, *61*, 3482.
[31] A. V. Kazantzis, Z. G. Chen, J. Th. M. De Hosson, *J. Mater. Sci.* **2013**, *48*, 7399.
[32] W. A. Soer, A. R. Chezan, J. Th. M. De Hosson, *Acta Mater.* **2006**, *54*, 3827.
[33] M. Legros, G. Dehm, E. Arzt, T. J. Balk, *Science* **2008**, *319*, 1646.
[34] Y. Amouyal, S. V. Divinski, Y. Estrin, E. Rabkin, *Acta Mater.* **2007**, *55*, 5968.
[35] G. Wilde, J. Ribbe, G. Reglitz, M. Wegner, H. Rösner, Y. Estrin, M. Zehetbauer, D. Setman, S. Divinski, *Adv. Eng. Mater.* **2010**, *12*, 758.
[36] L. E. Larsson, *Acta Metall.* **1967**, *15*, 35.
[37] K. Osamura, H. Okuda, S. Ochiai, *Scr. Metall.* **1985**, *19*, 1379.
[38] C. F. Yang, G. Sarkar, R. A. Fournelle, *Acta Metall.* **1988**, *36*, 1511.
[39] H.-G. Yi, J. K. Park, *Scr. Metall.* **1991**, *25*, 1799.
[40] C. P. Ju, R. A. Fournelle, *Acta Metall.* **1985**, *33*, 71.
[41] Z. Boumerzoug, L. Boudhib, A. Chala, *J. Mater. Sci.* **2005**, *40*, 3199.
[42] I. Manna, S. K. Pabi, W. Gust, *Int. Mater. Rev.* **2001**, *46*, 53.
[43] K. B. Rundman, J. E. Hilliard, *Acta Metall.* **1967**, *15*, 1025.
[44] A. Alhamidi, K. Edalati, Z. Horita, S. Hirosawa, K. Matsuda, D. Terada, *Mater. Sci. Eng. A* **2014**, *610*, 17.
[45] X. Sauvage, A. Dédé, A. Cabello Muñoz, B. Huneau, *Mater. Sci. Eng. A* **2008**, *491*, 364.
[46] G. Da Costa, F. Vurpillot, A. Bostel, M. Bouet, B. Deconihout, *Rev. Sci. Instrum.* **2005**, *76*, 013304.
[47] B. B. Straumal, A. A. Mazilkin, X. Sauvage, R. Z. Valiev, A. B. Straumal, A. M. Gusak, *Russ. J. Non-Ferr. Met.* **2015**, *56*, 44.
[48] K. Edalati, R. Miresmaeili, Z. Horita, H. Kanayama, R. Pippan, *Mater. Sci. Eng. A* **2011**, *528*, 7301.
[49] X. Sauvage, G. Wilde, S. V. Divinski, Z. Horita, R. Z. Valiev, *Mater. Sci. Eng. A* **2012**, *540*, 1.
[50] X. Sauvage, N. Enikeev, R. Valiev, Y. Nasedkina, M. Murashkin, *Acta Mater.* **2014**, *72*, 125.
[51] O. Renk, A. Hohenwarter, S. Wurster, R. Pippan, *Acta Mater.* **2014**, *77*, 401.
[52] X. Sauvage, Y. Nasedkina, *Diffusion Fundamentals Vol. 5 "Structure, Thermodynamics and Diffusion Properties of Grain Boundaries and Interfaces"* (Ed: V. Popov), Trans Tech Publications, Pfaffikon, Switzerland **2015**.

